2012 IEEE/RSJ International Conference on
Intelligent Robots and Systems
October 7-12, 2012. Vilamoura, Algarve, Portugal

The Cubli: A Cube that can Jump Up and Balance

Mohanarajah Gajamohan, Michael Merz, Igor Thommen and Raffaello D'Andrea

***Abstract*— This paper introduces the Cubli, a $15 \times 15 \times 15$ cm cube that can jump up and balance on a corner. Momentum wheels mounted on three faces of the cube (Fig. 1) rotate at high angular velocities and then brake suddenly, causing the Cubli to jump up. Once the Cubli has almost reached the corner stand-up position, controlled motor torques are applied to make it balance on its corner. This paper tracks the development of the Cubli's one dimensional prototype at ETH Zurich and presents preliminary results.**

I. Introduction

Inverted pendulum systems have a very rich history [1] and have been widely used to test, demonstrate and benchmark new control concepts and theories [2]. Furthermore, development of new control algorithms for the pendulum system itself is still an active area of research [3]–[5].

Compared to other 3D inverted pendulum test-beds [8], [9] the Cubli has two unique features. One is its relatively small footprint, (hence the name Cubli, which is derived from the Swiss German diminutive for "cube"). The other feature is its ability to jump up from a resting position without any external support, not only an interesting concept for the control engineer but also also an appealing demonstration for the general public.

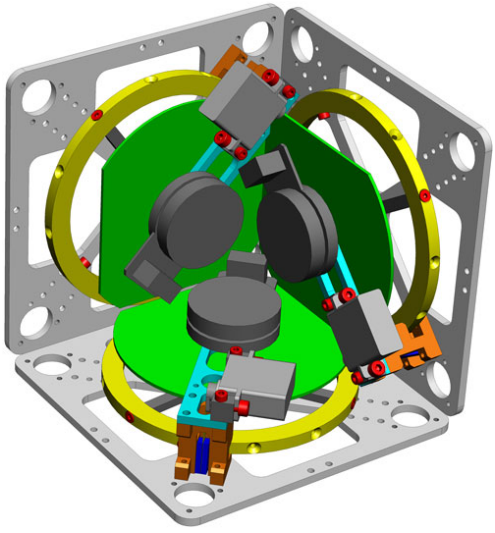

Fig. 1. The CAD drawing of the Cubli with covers removed

Fig. 2 shows the jumping up strategy of the Cubli. Initially the Cubli, lying flat on its face, will jump about its edge by instantaneously stopping one of its momentum wheels. Once the Cubli is balancing on its edge, the next two wheels are instantaneously stopped to make it stand on its corner. Finally, an inertial measurement unit (IMU) based state estimation is performed and the motor torques are precisely controlled to make the Cubli continue standing.

Whereas a relatively large portion of research tries to avoid impact or overcome the effects of it [10]–[12], only a small portion [13], including the Cubli, takes advantage of it. While a non-impulsive force is limited by the actuator torque limits, an impact gives forces that are well beyond the actuator limitations.

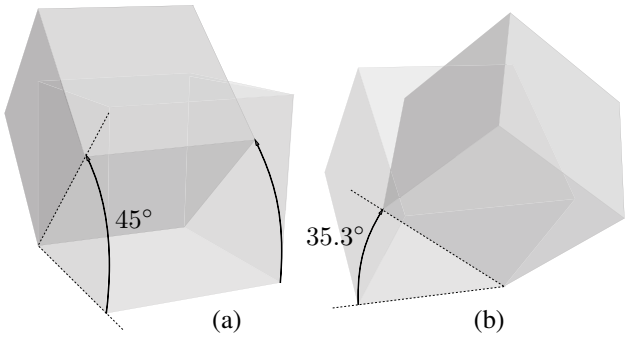

Fig. 2. The Cubli jump-up strategy: (a) Flat to Edge: Initially lying flat on its face, the Cubli jumps up to stand on its edge. (b) Edge to Corner: The Cubli goes from balancing about an edge to balancing on a corner.

Once complete, the Cubli will provide an inexpensive, open source test-bed with a relatively small footprint for research and education in estimation and control.

The three dimensional Cubli design started off with the following question:

> *How to build a 15 cm sided cube that can jump up and balance on its corner, using off-the-shelf motors, batteries, and electronic components ?*

Due to the structure's rigidity and off-the-shelf component constraint, only the momentum wheels allowed enough design flexibility in terms of mass distribution properties of the Cubli. Necessary angular velocities of the momentum wheels for jump-up were calculated assuming a perfectly inelastic collision between the wheels and the pendulum body.

Although high angular velocities of the wheels before braking can be reduced by increasing the wheel inertia, i.e., increasing wheel mass since the wheel size is constrained, this was not taken to the extreme since this will result in reduced recovery angles while balancing.

A gear chain between the wheel and the motor was avoided since it would not allow the high angular velocities for jump-up and would add extra weight and volume. Although the balancing maneuver, which requires high torques,

The authors are with the Institute for Dynamic Systems and Control, Swiss Federal Institute of Technology Zürich, Switzerland. The contact author is M. Gajamohan, e-mail: gajan@ethz.ch

was affected by the choice of no gear, the brushless DC motors were still able provide enough torque for recovery angles up to 7°.

The objective of this paper is to present the concept of the three dimensional Cubli along with the development of the one dimensional design, modelling, identification, and control. This paper also presents a control procedure to eliminate sensor offsets during the balance maneuver.

II. The One Dimensional Prototype

Fig. 3 illustrates the one dimensional prototype that was built to examine the feasibility and develop control algorithms for the Cubli. Similar momentum exchange wheel based inverted pendulum designs, except for the braking mechanism, can be found in [5]–[7]. The prototype consists of a square plastic plate that holds the momentum exchange wheel through the motor at its center and the braking mechanism at one of its corners. The dimension of the plastic plate matches the dimension of the proposed Cubli face, and it will be referred to hereafter as the pendulum body. The plate is attached to a bearing at the bottom that gives it a single degree of freedom to pivot around its corner on a horizontal plane.

A. System dynamics

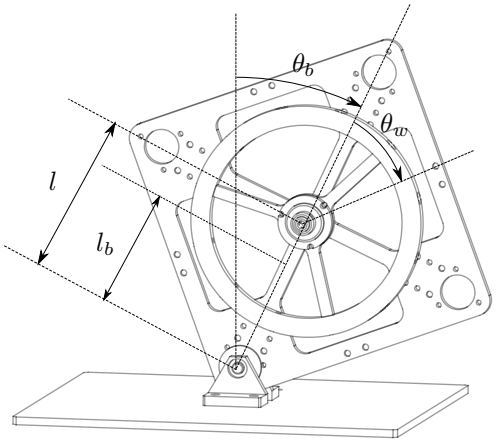

Fig. 3. Illustration of the one dimensional prototype consisting of a square plastic plate that holds the momentum exchange wheel through the motor at its center. The plate is attached to a bearing at the bottom.

Let θ_b denote the tilt angle of the pendulum body and θ_w represent the rotational displacement of the momentum wheel with respect to the pendulum body. The non-linear dynamics of the the setup shown in Fig. 3 is given by

$$\begin{aligned}\ddot{\theta}_b &= \frac{(m_b l_b + m_w l)\, g \sin\theta_b - T_m - C_b\dot{\theta}_b + C_w\dot{\theta}_w}{I_b + m_w l^2},\\ \ddot{\theta}_w &= \frac{\left(I_b + I_w + m_w l^2\right)\left(T_m - C_w\dot{\theta}_w\right)}{I_w\left(I_b + m_w l^2\right)}\\ &\quad - \frac{(m_b l_b + m_w l)\, g \sin\theta_b - C_b\dot{\theta}_b}{(I_b + m_w l^2)},\end{aligned} \tag{1}$$

where m_b, m_w are the pendulum body and wheel masses, I_b is moment of inertia of the pendulum body around the pivot point, I_w is the moment of inertia of the wheel and the motor rotor around the rotational axis of the motor, l is the distance between the motor axis and the pivot point, l_b is the distance between the center of mass of the pendulum body and the pivot point, $g = 9.81\ \mathrm{m\cdot s^{-2}}$ is the gravitational acceleration, T_m is the torque produced by the motor, and C_w, C_b are the dynamic friction coefficients of the pendulum body and wheel. Since we used a motor that allowed current set points controlled by an inner loop running at 10 kHz, the current-torque relationship can modelled as

$$T_m = K_m u, \tag{2}$$

where, $K_m = 25.1 \times 10^{-3}\ \mathrm{Nm\cdot A^{-1}}$ [14] is the torque constant of the brushless DC motor used and u is the current input.

B. Parameter identification

This subsection describes procedures for identifying the parameters in (1) that cannot be directly measured.

l_b was identified by freely hanging the pendulum body from different corners. To identify I_w and C_w, the momentum wheel was driven with different current steps, while pendulum body was rigidly fixed, and the time trace of $\dot{\theta}_w$ was recorded. A least squares fit with the measurements to

$$I_w\ddot{\theta}_w(t) = K_m u(t) - C_w\dot{\theta}_w(t)$$

gave I_w and C_w.

To identify I_b and C_b, after rigidly fixing the momentum wheel with the pendulum body the whole setup was hung upside down and was made to swing. A least squares fit with the measurements to

$$(I_b+I_w+m_w l^2)\ddot{\theta}_b(t) = -C_b\dot{\theta}_b(t)+(m_b l_b+m_w l)g\sin\theta_b(t)$$

gave I_b and C_b. The following table shows all the measured and identified parameters of the prototype:

l	$0.085\ \mathrm{m}$
l_b	$0.075\ \mathrm{m}$
m_b	$0.419\ \mathrm{kg}$
m_w	$0.204\ \mathrm{kg}$
I_b	$3.34 \times 10^{-3}\ \mathrm{kg\cdot m^2}$
I_w	$0.57 \times 10^{-3}\ \mathrm{kg\cdot m^2}$
C_b	$1.02 \times 10^{-3}\ \mathrm{kg\cdot m^2\cdot s^{-1}}$
C_w	$0.05 \times 10^{-3}\ \mathrm{kg\cdot m^2\cdot s^{-1}}$

C. Braking mechanism

Fig. 4 shows the current iteration of the braking mechanism where an RC servo is used to quickly collide a metal barrier with the bolt head attached to the momentum wheel. The metal barrier and the RC servo are connected using a thin metal sheet to ensure that most of the impact is taken by the metal barrier. Furthermore, the design guarantees that the metal barrier is easily replaceable. The RC servo-based braking mechanism had several advantages over the initial solenoid-based braking mechanism in terms of weight (a reduction of 39g), power and durability.

To test the durability of the stopping mechanism, and to select the appropriate material for the metal barrier, several

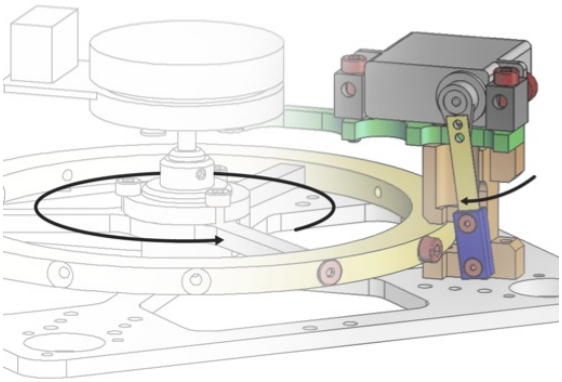

Fig. 4. The CAD drawing of the RC servo-based braking mechanism: An RC servo is used to quickly collide a metal barrier (blue) with the bolt head (red) attached to the momentum wheel.

jump up trials were done with additional steel plates attached to the pendulum body such that the mass and the inertia properties are equal to the full Cubli's face to edge jump as shown in Fig. 8.

D. Electronics and software

The power, computation and control components were not mounted on the one dimensional prototype to avoid making the first prototype too complex. Figure 5 shows the overall electronics setup except for the power, which was provided by a constant voltage supply.

We selected the STM3210E evaluation board, (which houses a Cortex-M3 clocked at 72 MHz) from STMicroelectronics as the main controller for its rapid prototyping and readily available community support. The IMU comprised of a 3-axis accelerometer, ADXL345 from Analog Devices, and a 3-axis rate-gyro using the IDG-500/ISZ-500 series from InvenSense. The two IMUs, mounted on the pendulum body as shown in Fig. 6, was connected to the evaluation board using two separate Serial Peripheral Interface (SPI) buses.

A 50 W brushless DC motor, EC-45-flat, from Maxon Motor AG was selected to drive the momentum wheels for their high energy density as compared to the brushed DC motors. Embedded hall sensors of the motor were used for wheel speed, $\dot{\theta}_w$, sensing. The motor was controlled using an off-the-shelf digital four quadrant motor controller, EPOS2 50/5, from Maxon. The CANopen protocol was used for the communication between the motor controller and the evaluation board. Note that for the full Cubli, a miniature version of the above controller, DEC module 36/2, will be used.

The RC Servo, HSG-5084MG, of the braking mechanism was driven by the PPM signals from the evaluation board. For debugging purposes a high speed rotary magnetic encoder, RE36 [15], was used to measure θ_b and was connected to the timing/counter unit of the evaluation board.

The STM32 port of the FreeRTOS scheduler was used in the software framework for its prioritized multitasking functionalities provided by a scheduler, and for the small footprint of the binary kernel image (4 kB). A completely open source and a free development environment for embedded systems named ODeV [16], based on the Eclipse IDE, was used for the software development.

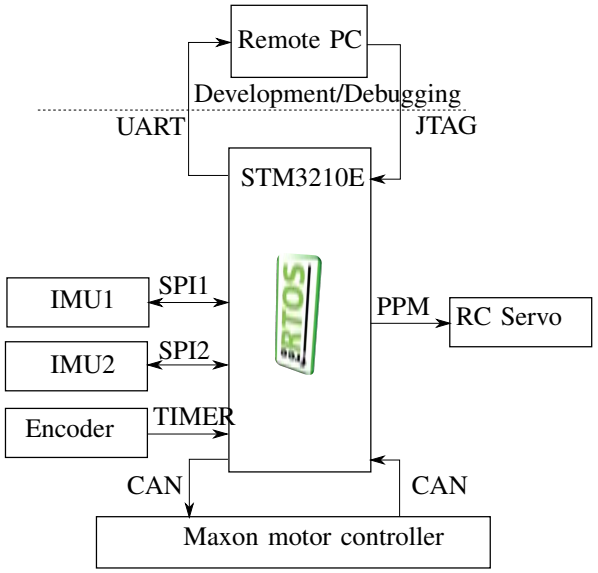

Fig. 5. The schematic diagram of the electronics setup

III. Estimation and Control

A. IMU-based tilt angle estimation and IMU calibration

To estimate the tilt angle θ_b of the pendulum body, a purely accelerometer-based tilt estimation was implemented using two accelerometers. Note that this method can be extended [9] to the 3D tilt estimation of the Cubli.

Two accelerometers were placed along the diagonal of the pendulum body at distances r_i, $i = 1, 2$ from the pivot point as shown in Fig. 6. The two most sensitive measurement axis ${}_b\vec{e}_{x_i}$, ${}_b\vec{e}_{y_i}$ were placed on the pendulum body plane with ${}_b\vec{e}_{x_i}$ pointing towards tangential and ${}_b\vec{e}_{y_i}$ towards the radial direction. With this setup, the measured acceleration of the accelerometer i, $i = 1, 2$, with respect to the accelerometer frame is given by

$$ {}_{ai}m := (r_i\ddot{\theta}_b + g\sin\theta_b, -r_i\dot{\theta}_b^2 - g\cos\theta_b, 0), \quad i = 1, 2. $$

The dynamic terms can be eliminated by

$$ \begin{aligned} {}_{a1}m - \mu_{a2}m &= ((1-\mu)g\sin\theta_b, -(1-\mu)g\cos\theta_b, 0), \\ &=: (m_x, m_y, 0), \end{aligned} $$

where $\mu = r_1/r_2$ and the estimated tilt angle of the pendulum body is given by $\hat{\theta}_b := \tan^{-1}(-m_x/m_y)$.

The mechanical placement errors of the accelerometers were identified by the following procedure:

- Record the accelerometer measurements when the pendulum body is fixed ($\dot{\theta}_b = 0$) at various tilt angles $\theta_b \in [-\pi/4, +\pi/4]$.
- Do principle component analysis to find the rotational plane with respect to the accelerometer frame.
- Calculate the orientation offset by projecting the measurements into the rotational plane and defining a reference frame.

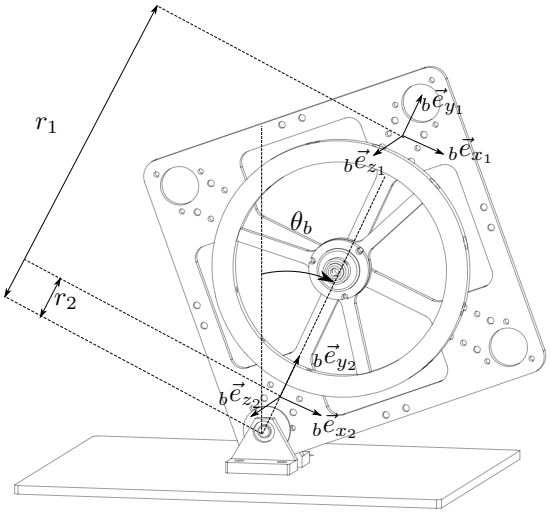

Fig. 6. Illustration of the tilt angle estimation setup using two accelerometers: Two accelerometers were placed along the diagonal of the pendulum body at distances r_i, $i = 1, 2$ and the ratio between the distances is used to eliminate the dynamic terms, $r_i\ddot{\theta}_i$, $r_i\dot{\theta}_i^2$, $i = 1, 2$ from the measurements.

B. Jumping Up

Assuming a perfectly inelastic collision i.e., a zero coefficient of restitution, the angular velocity ω_w of the momentum wheel required for jump-up is calculated using: (1) The conservation of angular momentum during the impact

$$I_w\omega_w = (I_w + I_b + m_w l^2)\omega_b,$$

where ω_b is the angular velocity of the pendulum body after the impact. (2) The conservation of energy after the impact ($\theta_b = \pi/4$) and until the pendulum body reaches the top ($\theta_b = 0$)

$$\frac{1}{2}(I_w + I_b + m_w l^2)\omega_b^2 = (m_b l_b + m_w l)g(1 - \frac{1}{\sqrt{2}}).$$

Eliminating ω_b from both equations gives

$$\omega_w^2 = (2 - \sqrt{2})\frac{(I_w + I_b + m_w l^2)}{I_w^2}(m_b l_b + m_w l)g. \quad (3)$$

The uncertainties in the parameters or a non zero coefficient of restitution can make ω_w deviate from the above calculated value. In this case a simple bisection-based trial and error learning procedure can be applied to learn the required ω_w, exploiting the monotic relationship between θ_b achieved after the impact and ω_w. The ω_w given by (3) can be used as the initial condition in this case. After the collision, once the pendulum body has arrived near the equilibrium position, an LQR based controller, explained in the following section, will start balancing the system.

C. Balancing control

Linearizing (1) around $(\theta_b,\ \dot{\theta}_b, \dot{\theta}_w) = (0, 0, 0)$ gives

$$\dot{x}(t) = Ax(t) + Bu(t). \quad (4)$$

where $x := (\theta_b,\ \dot{\theta}_b, \dot{\theta}_w)$,

$$A := \begin{bmatrix} 0 & 1 & 0 \\ \frac{(m_b l_b + m_w l)g}{I_b + m_w l^2} & -\frac{C_b}{I_b + m_w l^2} & \frac{C_w}{I_b + m_w l^2} \\ -\frac{(m_b l_b + m_w l)g}{I_b + m_w l^2} & \frac{C_b}{I_b + m_w l^2} & -\frac{C_w((I_b + I_w + m_w l^2)}{I_w(I_b + m_w l^2)} \end{bmatrix},$$

$$\text{and} \quad B := \begin{bmatrix} 0 \\ -\frac{K_m}{I_b + m_w l^2} \\ \frac{K_m(I_b + I_w + m_w l^2)}{I_w(I_b + m_w l^2)} \end{bmatrix}.$$

A 20 ms sampling time was selected for the digital control, considering the open loop unstable pole of (4) (637.4 ms) and a safety factor of 30. Using this sampling time the continuous time system given by (4) was discretized using zero-order hold and the resulting discrete time model is given by

$$x[k+1] = A_d x[k] + B_d u[k], \quad k \in \mathbb{N}_0, \quad (5)$$

where A_d and B_d are the discrete-time counterparts of the continuous time state matrix A and input matrix B. For the sake of simplicity we use the same notation to represent the continuous and discrete time versions of the state x and input u.

Using the above discrete time model, a Linear Quadratic Regulator (LQR) feedback controller of the form

$$u[k] = -K_d(\hat{\theta}_b[k], \hat{\dot{\theta}}_b[k], \hat{\dot{\theta}}_w[k]) \quad (6)$$

was designed, where $K_d = (K_{d1}, K_{d2}, K_{d3})$ is the LQR feedback gain that minimizes the cost function

$$J(u) := \sum_{k=1}^{\infty} x^{\mathrm{T}}[k]Qx[k] + u^{\mathrm{T}}[k]Ru[k], \quad Q \geqslant 0, R > 0,$$

$\hat{\dot{\theta}}_b$ is the angular velocity estimate of the body from the rate gyro, and $\hat{\dot{\theta}}_w$ is the angular velocity estimate of the momentum wheel from the hall sensors. Fig. 9 illustrates the balancing performance under (6). As it can be seen from the plot, the estimated state of the system converges to $(\theta_b,\ \hat{\dot{\theta}}_b, \hat{\dot{\theta}}_w) = (-0.058, 0.0, 37.0)$. This behavior can be explained by the following property of the system:

$$(I_3 - A_d + B_d K_d)^{-1} B_d \quad = \quad (0, 0, \frac{K_m}{C_w + K_{d3} K_m}), \quad (7)$$
$$C_w + K_{d3} K_m \neq 0,$$

where I_3 is the identity matrix of size 3. The physical interpretation of this property is that if A_d, B_d, and K_d gives a stable system, any constant offset in the measurement will result in a non-zero wheel velocity at steady state. Using the readings from the absolute encoder attached to the pendulum body at the pivot point, we localized the offset to the offset in the tilt angle and redefined the tilt angle estimate as

$$\hat{\theta}_b := \tan^{-1}(-m_x/m_y) + d = \theta_b + d, \quad d \in \mathbb{R}.$$

To automatically eliminate the above constant tilt angle offset, the discrete time system given in (5) was extended

by introducing a low-pass filter with state $x_f[k]$ and the following dynamics:

$$x_f[k+1] = (1-\alpha)x_f[k] + \alpha\hat{\theta}_b[k], \quad x_f[0] = 0, \tag{8}$$

where $\alpha \in (0,1)$ and the controller was modified to

$$u[k] = -K_d(\hat{\theta}_b[k] - x_f[k], \hat{\dot{\theta}}_b[k], \hat{\dot{\theta}}_w[k]). \tag{9}$$

The closed loop system given by (5), (8) and (9) is stable with $\alpha = 0.02$. Now, let $((\bar{\theta}_b,\ \bar{\dot{\theta}}_b, \bar{\dot{\theta}}_w) =: \bar{x}, \bar{x}_f)$ denote the steady states of the system, which is the solution to

$$\begin{aligned} \bar{x} &= A_d\bar{x} - B_dK_d\bar{x} - B_dK_{d1}(d - \bar{x}_f) \\ \bar{x}_f &= (1-\alpha)\bar{x}_f + \alpha(\bar{\theta}_b + d). \end{aligned}$$

This, with (8), gives

$$\begin{aligned} \bar{x} &= -(I - A_d + B_dK_d)^{-1}B_dK_{d1}(d - \bar{x}_f) \\ &= -\begin{bmatrix} 0 \\ 0 \\ \frac{K_mK_{d1}}{C_w + K_{d3}K_m} \end{bmatrix}(d - \bar{x}_f) \qquad (10) \\ \bar{x}_f &= (1-\alpha)\bar{x}_f + \alpha(\bar{\theta}_b + d). \qquad (11) \end{aligned}$$

Finally, (10) and (11) gives $(\bar{\theta}_b,\ \bar{\dot{\theta}}_b, \bar{\dot{\theta}}_w, \bar{x}_f) = (0,0,0,d)$ showing that the system reaches the desired equilibrium state and the filter state x_f converges to the tilt angle offset d with the proposed controller. Although the zero mean sensor noise on the measurements were avoided in the formulation for the sake of simplicity, the results are still valid under this type of noise.

Fig. 10 shows a balancing experiment with the offset correction. The estimated states $(\hat{\theta}_b,\ \hat{\dot{\theta}}_b, \hat{\dot{\theta}}_w)$ converge to $(-0.058, 0, 0)$ and the filter state x_f converges to the offset value -0.058 rad. Fig. 11 shows a balancing experiment where the system was externally disturbed at time $t = 26$[s]. Furthermore, fig 12 shows the full jump-up and balancing maneuver starting from rest at $\theta_b = -\pi/4$.

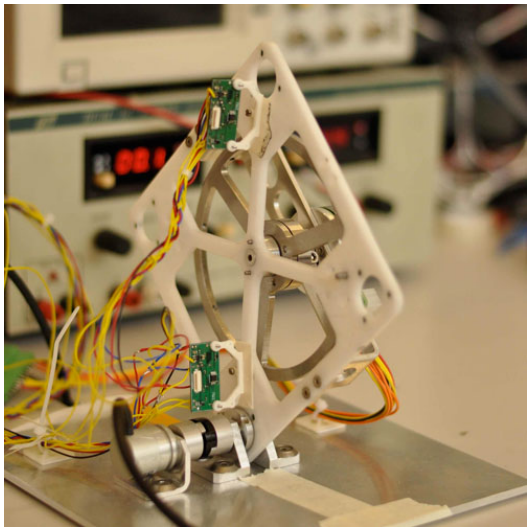

Fig. 7. A picture of the first one dimensional prototype while balancing

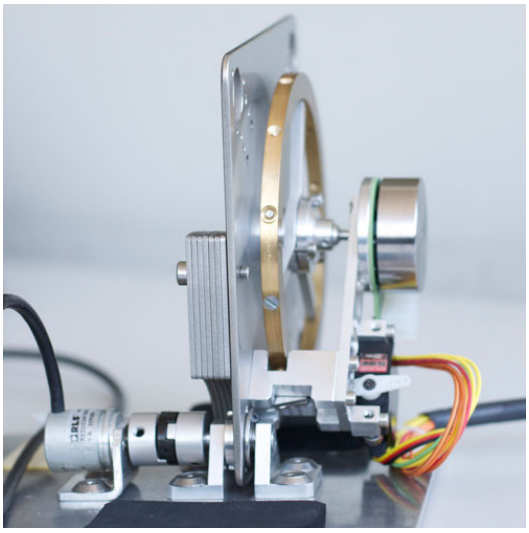

Fig. 8. The picture shows another one dimensional prototype that was built with a metal pendulum body with extra masses (on the left side of the pendulum body) to test the durability of the braking mechanism. With all the weights attached, it resembles the full Cubli's flat to edge jump, the most critical jump for the Braking mechanism, in terms of mass and inertia.

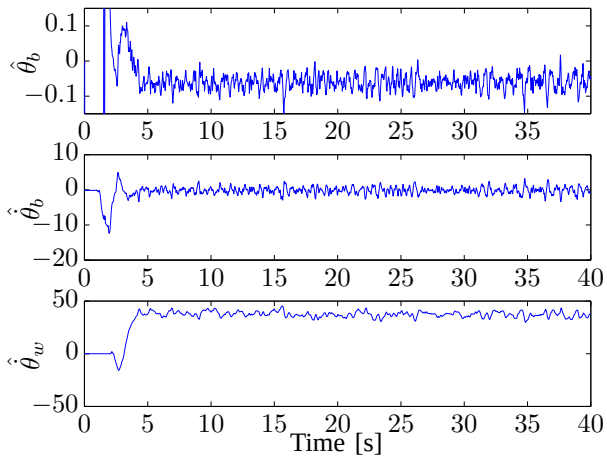

Fig. 9. Time traces of the one dimensional prototype's estimated states during a balancing run with no offset correction on the body tilt angle. The estimated state of the system converges to $(\hat{\theta}_b,\ \hat{\dot{\theta}}_b, \hat{\dot{\theta}}_w) = (-0.058, 0.0, 37.0)$.

IV. Conclusion and Future Work

This paper presented the Cubli, a unique 3D inverted pendulum that jumps up using a self-generated impact and balances using the exchange of angular momentum. The one dimensional prototype has demonstrated various important aspects of the system, including: the hardware, jump-up using impact, accelerometer-based tilt estimation, control, and software. The Cubli is currently undergoing its second iteration with on-board electronics and power. Once successful, three copies of the one dimensional prototype will be put together to produce the 3D version (See Fig. 1). These results will be presented in future work.

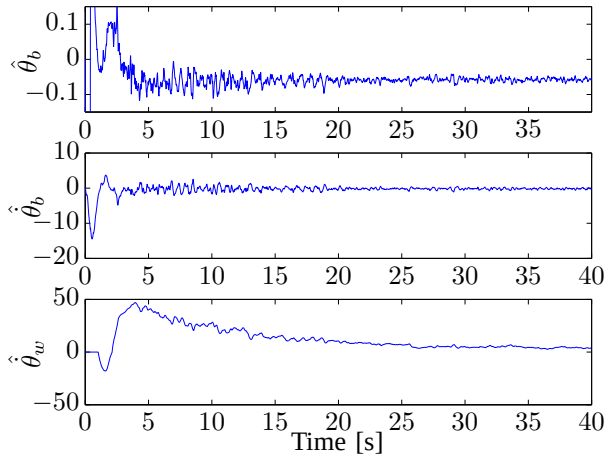

Fig. 10. Time traces of the one dimensional prototype's estimated states during a balancing run with offset correction on the body tilt angle. The estimated state of the system converges to $(\hat{\theta}_b,\ \dot{\hat{\theta}}_b, \dot{\hat{\theta}}_w) = (-0.058, 0.0, 0.0)$.

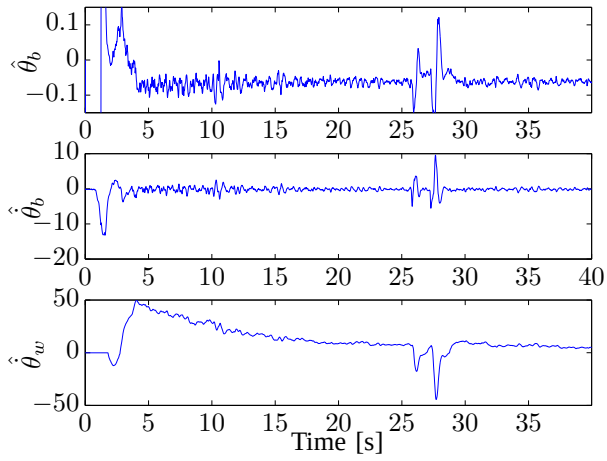

Fig. 11. Time traces of the one dimensional prototype's estimated states during a balancing run with offset correction on the body tilt angle and an external disturbance at time $t = 26$ [s].

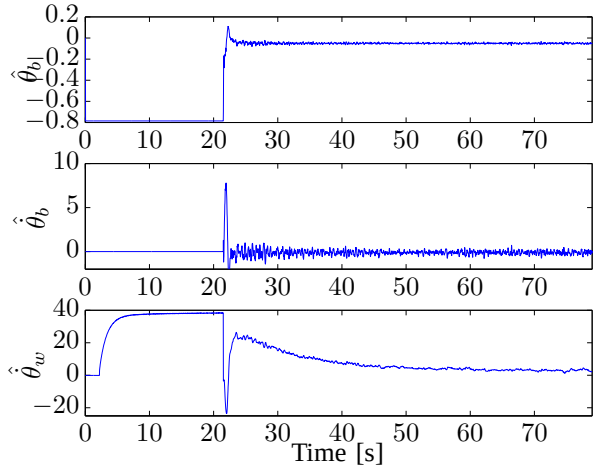

Fig. 12. Time traces of the one dimensional prototype's estimated states during a jump-up and balance maneuver.

V. Acknowledgements

The Authors would like to thank Sebastian Trimpe and Raymond Oung for all the support and discussions sharing their experience on building the Balancing Cube [9] and the Distributed Flight Array [17]. Furthermore, the authors would like to extend their gratitude to Philipp Reist for the idea of the impact based jump-up strategy, Carolina Flores for the graphics, and Tobias Widmer for helping with the experiments.

References

[1] A. Stephenson, "On a new type of dynamical stability," *Proceedings: Manchester Literary and Philosophical Society*, vol. 52, pp. pp. 1–10, 1908.

[2] P. Reist and R. Tedrake, "Simulation-based lqr-trees with input and state constraints," in *Robotics and Automation (ICRA), 2010 IEEE International Conference on*, may 2010, pp. 5504 –5510.

[3] D. Alonso, E. Paolini, and J. Moiola, "Controlling an inverted pendulum with bounded controls," in *Dynamics, Bifurcations, and Control*, ser. Lecture Notes in Control and Information Sciences. Springer Berlin / Heidelberg, 2002, vol. 273, pp. 3–16.

[4] M. V. Bartuccelli, G. Gentile, and K. V. Georgiou, "On the stability of the upside-down pendulum with damping," *Proceedings: Mathematical, Physical and Engineering Sciences*, vol. 458, no. 2018, pp. pp. 255–269, 2002.

[5] J. Meyer, N. Delson, and R. de Callafon, "Design, modeling and stabilization of a moment exchange based inverted pendulum," in *15h IFAC Symposium on System Identification, Saint-Malo, France*, 2009, pp. 462 – 467.

[6] B. Andrievsky, "Global stabilization of the unstable reaction-wheel pendulum," *Automation and Remote Control*, vol. 72, pp. 1981–1993, 2011. [Online]. Available: http://dx.doi.org/10.1134/S0005117911090189

[7] A. Beznos, A. Grishin, A. Lenskij, D. Okhotsimskij, and A. Formal'skij, "A flywheel use-based control for a pendulum with a fixed suspension point," . , no. 1, pp. 27–38, 2004.

[8] D. Bernstein, N. McClamroch, and A. Bloch, "Development of air spindle and triaxial air bearing testbeds for spacecraft dynamics and control experiments," in *American Control Conference, 2001. Proceedings of the 2001*, vol. 5, 2001, pp. 3967 –3972 vol.5.

[9] S. Trimpe and R. D'Andrea, "Accelerometer-based tilt estimation of a rigid body with only rotational degrees of freedom," in *Robotics and Automation (ICRA), 2010 IEEE International Conference on*, May 2010, pp. 2630 –2636.

[10] D. N. Nenchev and K. Yoshida, "Impact analysis and post-impact motion control issues of a free-floating space robot subject to a force impulse," *IEEE Transactions on Robotics and Automation*, vol. 15, no. 3, pp. 548–557, 1999. [Online]. Available: http://ieeexplore.ieee.org/lpdocs/epic03/wrapper.htm?arnumber=768186

[11] T.-J. Tarn, Y. Wu, N. Xi, and A. Isidori, "Force regulation and contact transition control," *Control Systems, IEEE*, vol. 16, no. 1, pp. 32 –40, feb 1996.

[12] P. Pagilla and B. Yu, "An experimental study of planar impact of a robot manipulator," *Mechatronics, IEEE/ASME Transactions on*, vol. 9, no. 1, pp. 123 –128, march 2004.

[13] A. Konno, T. Myojin, T. Matsumoto, T. Tsujita, and M. Uchiyama, "An impact dynamics model and sequential optimization to generate impact motions for a humanoid robot," *Int. J. Rob. Res.*, vol. 30, no. 13, pp. 1596–1608, Nov. 2011. [Online]. Available: http://dx.doi.org/10.1177/0278364911405870

[14] (2012, Feb) Maxon motor ag, maxon motor catalog, ec-45-flat. [Online]. Available: http://www.maxonmotor.com/

[15] (2012, Feb) Rotary and linear motion sensors (rls), re36. [Online]. Available: http://www.rls.si/document/RE36D01.pdf

[16] S. Oliveri. (2012, Feb) Open development environment for embedded application. [Online]. Available: http://www.stf12.org/developers/ODeV.html

[17] R. Oung and R. DAndrea, "The distributed flight array," *Mechatronics*, vol. 21, no. 6, pp. 908 – 917, 2011. [Online]. Available: http://www.sciencedirect.com/science/article/pii/S095741581000139X